Fast Track

Jaesool Shim[1,2]
Prashanta Dutta[1]
Cornelius F. Ivory[3]

[1]School of Mechanical and Materials Engineering, Washington State University, Pullman, WA, USA
[2]School of Mechanical Engineering, Yeungnam University, Gyeongsan, Korea
[3]School of Chemical Engineering and Bioengineering, Washington State University, Pullman, WA, USA

Received November 9, 2008
Revised December 8, 2008
Accepted December 13, 2008

Research Article

Dispersion of protein bands in a horseshoe microchannel during IEF

Ampholyte-based IEF is simulated for a 2-D horseshoe microchannel. The IEF model takes into account ionic-strength-dependent mobility corrections for both proteins and ampholytes. The Debye–Huckel–Henry model is employed to correct the protein mobilities and the Onsager–Debye–Huckel model is used to obtain effective mobilities of ampholytes from their limiting mobility. IEF simulations are conducted in the presence of 25 ampholytes ($\Delta pK = 3.0$) within a pH range of 6–9 under an electric field of 300 V/cm and using four proteins (p*I*s = 6.49, 7.1, 7.93 and 8.6) focused in a 1-cm-long microchannel. The numerical results show that the concentrations of proteins and ampholytes are different when mobility corrections are considered but that the focusing positions remain the same regardless of mobility corrections. Our results also demonstrate that, unlike linear electrophoresis in which the bands deform significantly as they traverse a bend, during the transient portion of IEF racecourse dispersion is mitigated by focusing and, at focused-state, those bands that focus in the bend show no radial concentration dependence, *i.e.* they completely recover from racecourse dispersion, even within a tight turn.

Keywords:
Band dispersion / Horseshoe microchannel / IEF / Protein
DOI 10.1002/elps.200800728

1 Introduction

Microscale electrophoretic techniques have been successfully demonstrated due to their shorter processing time, high resolution, low reagent consumption and overall cost-effectiveness. These include IEF [1–4], ITP [5–7], ZE [8–9] and CE [10]. Recently, multi-dimensional separation techniques such as IEF–ZE [11], IEF–CE [12], ITP–ZE [13] and ITP–IEF [14] have been reported in microchip to enhance separation efficiency of large numbers of proteins. As 2-D separation techniques are integrated onto small microchips, one has to design appropriate channel configurations using complex geometries such as cross-channels, T-channels, dog-leg or horseshoe channels in order to obtain high-resolution separations. One of the undesirable consequences of complex channel design for a compact microfluidic chip is the dispersion of solute band in turns and junctions [15]. Dispersion limits the efficiency of separation in bioanalytical processes as demonstrated in a number of analytical and computational studies in microfluidic devices [16–18].

The primary sources of solute band dispersions are Joule heating [19], extended electric double-layers [20] and complex channel shapes such as dog legs [15] or cross-channels [12]. In a traditional, large-scale separation, Joule heating effect cannot be neglected because high voltages induce non-uniform temperature in a separation channel [21, 22]. However, in a microfluidic chip, Joule heating is not a major source of dispersion because of the large channel surface-to-volume ratio [23]. Dispersion due to extended double-layers can be very high in a nanofluidic application [20], but its contribution will be negligible in the case of a microfluidic channel (10–100 μm) [18]. However, dispersion due to complex channel shapes is very important in all devices, especially in an integrated lab-on-a-chip device because multi-dimensional separations require complex geometries.

The basic mechanism of dispersion in curved channels is described thoroughly for CE [18]. Culbertson *et al.* [16] reported dispersion sources for turns on microchips in synchronized cyclic electrophoresis. They developed an analytical expression for band dispersion in a curved chan-

Correspondence: Dr. Prashanta Dutta, School of Mechanical and Materials Engineering, Washington State University, PO Box 642920, Pullman 99164, WA, USA
E-mail: dutta@mme.wsu.edu
Fax: +1-509-335-4662

nel in terms of channel width, mean radius, turn angle and Peclet number. Griffiths and Nilson [17] reported analytical and numerical results for band broadening in a microchannel turn and adjoining straight channel segments for electrokinetic species transport. They considered transport of a single charged species in a stationary phase. They concluded that dispersive band broadening is proportional to the product of the turn angle and the Peclet number at low Peclet numbers, but independent of the Peclet number when the Peclet number is large. More recently, Paschkewitz *et al.* [24] demonstrated both theoretically and experimentally that during ITP around moderate bends, small fluorescent dyes would form and maintain their ITP zones, suffering only mild deformation, but that the solute would preferentially gather at one or both walls as it coursed around the bend and would then recover entirely soon after it entered a straight run. Although the ability of ITP to recover from a discrete dispersive perturbation has long been known, the collection of sample at the walls in a turn was unexpected and suggested to us that this might also happen when during IEF. In particular, it seemed possible that this phenomenon might persist in an IEF band that happened to focus inside a bend.

In this study, the dispersion of protein bands is studied in a horseshoe channel for ampholyte-based IEF. Mobility corrections for proteins and ampholytes are included in the model because the mobility of both large molecules (proteins) and small molecules (ampholytes) varies with ionic strength during IEF [25]. We particularly show dispersion behavior of proteins in IEF and discuss the differences between linear electrophoretic transport (such as ZE and CE) and non-linear IEF in a horseshoe microchannel.

2 Theory

The general mathematical model for multi-dimensional IEF is presented in our earlier publications [26, 27]. In this section, a brief review of the governing equations used in the numerical model is presented. The ampholyte-based IEF model is primarily based on mass conservation, charge conservation and electroneutrality equations. In IEF, the concentration of the ith component (C_i) is obtained by summing all J_i+1 species (S_{ij}) in the system with a total of J_i dissociable groups, *i.e.*

$$C_i = \sum_{j=1}^{J_i+1} S_{ij} \tag{1}$$

The ith components include all ampholytes and proteins. The effective mobility ($\langle \mu_i \rangle$) and effective valance ($\langle z_i \rangle$) of a component, C_i, can be defined as follows:

$$\langle \mu_i \rangle = \frac{\sum_{j=1}^{J_i+1} \mu_{ij} S_{ij}}{C_i} \tag{2}$$

$$\langle z_i \rangle = \frac{\sum_{j=1}^{J_i+1} z_{ij} S_{ij}}{C_i} \tag{3}$$

where μ_{ij} and z_{ij} are the electrophoretic mobility and the valence of the J_i+1 species that make up each ith component in the system, respectively.

The mass conservation equation for each component (C_i) is obtained by summing the conservation equations for the J_i+1 species to yield

$$\frac{\partial C_i}{\partial t} + \nabla \cdot \left[\langle \mu_i \rangle \vec{E}\, C_i - D_i \nabla C_i \right] = \frac{\partial C_i}{\partial t} + \nabla \cdot \left[\bar{\omega}_i \langle z_i \rangle \vec{E}\, C_i - D_i \nabla C_i \right] = 0 \tag{4}$$

where $\vec{E}$ is the electric field ($-\Delta\phi$) and D_i is the diffusion coefficient of component i. If the dissociation reactions are fast, we also have J_i algebraic relations for equilibrium constants (K_{ij}) among the component i species,

$$K_{ij} = \frac{C_{H^+} S_{ij}}{S_{ij+1}} \tag{5}$$

which must be solved together with Eq. (4) for each component.

The charge conservation equation is expressed as

$$\nabla \cdot \left[\sum_{i=1}^{M} \sum_{j=1}^{J_i+1} z_{ij} \mu_{ij} S_{ij} \vec{E} + (\mu_{H^+} C_{H^+} - \mu_{OH^-} C_{OH^-}) \vec{E} \right] = \sum_{i=1}^{M} \sum_{j=1}^{J_i+1} z_{ij} D_{ij} \nabla^2 S_{ij} + D_{H^+} \nabla^2 C_{H^+} - D_{OH^-} \nabla^2 C_{OH^-} \tag{6}$$

where M is the number of components (ampholytes and proteins). The subscripts H^+ and OH^- represent hydronium and hydroxyl ions, respectively. For ampholyte-based IEF, the electroneutrality constraint must be satisfied over the channel as,

$$C_{H^+} - \frac{K_W}{C_{H^+}} = -\sum_{i=1}^{M} \langle z_i \rangle C_i \tag{7}$$

where K_W is the equilibrium constant for water.

2.1 Mobility corrections for ampholytes

In ampholyte-based IEF, ampholytes play an important role in pH formation. The effective mobility of the ith amphoteric component ($\langle \mu_i \rangle$) depends on the ionic strength of the buffer. For a biprotic ampholyte (three charge states; $j = 1^+, 0, 1^-$), the dissociation–association relations can be described as,

$$\begin{aligned} S_{i1^+} &\leftrightarrow S_{i0} + H^+ \\ S_{i0} &\leftrightarrow S_{i1^-} + H^+ \end{aligned} \tag{8}$$

For dilute aqueous solutions (less than 100 mM of ionic strength), the effective mobility, ($\langle \mu_i \rangle$) can be expressed as [28]

$$\langle \mu_i \rangle = \frac{\mu_{i1^+} 10^{pK_{i1}^{mix} - pH} + \mu_{i1^-} 10^{pH - pK_{i2}^{mix}}}{1 + 10^{pK_{i1}^{mix} - pH} + 10^{pH - pK_{i2}^{mix}}} \tag{9}$$

where $pK_{i1}^{mix} = -\log_{10} K_{i1}^{mix}$, $pK_{i2}^{mix} = -\log_{10} K_{i2}^{mix}$ and K_{i1}^{mix} and K_{i2}^{mix} are the mixed equilibrium constants [29]. The corrected mobility of species (μ_{i1} and μ_{i1^-}) is given by the Onsager–Debye–Huckel equation as [28, 29]

$$\mu_{i1^+} = \mu_{i1^+}^0 - \left(\mu_{i1^+}^0 z_{i1^+}|z_{i1^-}|B_1\frac{q_i}{1+\sqrt{q_i}} + B_2 z_{i1^+}\right) \times \frac{\sqrt{I_s}}{1+1.5\sqrt{I_s}} \quad (10a)$$

$$\mu_{i1^-} = \mu_{i1^-}^0 - \left(\mu_{i1^-}^0 z_{i1^+}|z_{i1^-}|B_1\frac{q_i}{1+\sqrt{q_i}} + B_2|z_{i1^-}|\right) \times \frac{\sqrt{I_s}}{1+1.5\sqrt{I_s}} \quad (10b)$$

where μ_{ij}^0 is the limiting mobility at the infinite dilution, I_s is the ionic strength ($I_s = \frac{1}{2}\sum_{i=1}^{M}\sum_{j=1}^{J_i+1} z_{ij}^2 S_{ij}$), and B_1 and B_2 are constants [29]. For aqueous solutions at 25°C, $B_1 = 0.7817\ \mathrm{mM}^{-1/2}$ and $B_2 = 3.138E\text{-}04\ \mathrm{cm^2\,s^{-1}\,mM^{-1/2}}$. The parameter q_i is defined as

$$q_i = \frac{z_{i1^+}|z_{i1^-}|}{z_{i1^+}+|z_{i1^-}|}\left(\frac{\mu_{i1^+}^0+\mu_{i1^-}^0}{|z_{i1^-}|\mu_{i1^+}^0 + z_{i1^+}\mu_{i1^-}^0}\right) \quad (11)$$

The mixed equilibrium constants can be obtained from the equilibrium constants as

$$K_{i1}^{mix} = \frac{\gamma_{i1^+}K_{i1}}{\gamma_{i0}} \quad (12)$$

$$K_{i2}^{mix} = \frac{\gamma_{i0}K_{i2}}{\gamma_{i1^-}} \quad (13)$$

where γ_{ij} is the activity coefficient, and it is related to the ionic strength as

$$\gamma_{i0} = 1 \quad (14a)$$

$$\log\gamma_{i1^\pm} = \frac{-Az_{i1^\pm}^2\sqrt{I_s}}{1+1.5\sqrt{I_s}} + 0.1I_s z_{i1^\pm}^2 \quad (14b)$$

where A is a constant with value of $A = 0.5085\ \mathrm{mM}^{-1/2}$ in aqueous solution at 25°C.

2.2 Mobility corrections for proteins

Like small ions or ampholytes, the absolute mobility of macromolecules such as proteins depends on the ionic strength. Mosher *et al.* calculated ionic-strength-dependent protein mobilities using Debye–Huckel–Henry theory [30]. In this study, we have adopted the Debye–Huckel–Henry theory to correct the protein mobility during IEF. According to that model, the corrected mobility of a protein can be expressed as [31]

$$\overline{\omega}_i = \frac{ef(\kappa r_i)}{6\pi\eta r_i(1+\kappa r_i)} \quad (15)$$

where e is the electron charge, η is the viscosity of the fluid, κ is the inverse Debye length (m^{-1}), r_i is the protein radius (m) and f is Henry's function.

The inverse Debye length is defined by the following equation:

$$\kappa = F\sqrt{\frac{2}{\varepsilon\varepsilon_0 RT}I_s} \quad (16)$$

where ε is the dielectric constant of the fluid, ε_0 is the permittivity of free space, R is the universal gas constant and T is the absolute temperature. In addition, the equation used for Henry's function is obtained by fitting data [32] as

$$f(\kappa r_i) = \frac{[5 - erf(\frac{5}{4}[0.10392\{\log(\kappa r_i)\}^2 - 1.10094\log(\kappa r_i) + 0.99302)]}{4} \quad (17)$$

The radius of the protein is calculated from Stokes equation as

$$r_i = \frac{k_B T}{6\pi\eta D_i} \quad (18)$$

where k_B is the Boltzmann constant. For spherical particles, Henry's function (Eq. (17)) has a minimum value of 1.0 in infinitely dilute media (Huckel approximation), whereas it has a maximum value of 1.5 in highly polar media (Smoluchowski approximation).

3 Computational model and assumptions

The set of equations that must be simultaneously solved consists of mass conservation equations (Eq. (4)), the charge conservation equation (Eq. (6)), and an electroneutrality condition (Eq. (7)) presented in the theory section. The concentration of hydronium is determined from the electroneutrality equation, whereas the protein and ampholyte concentrations are obtained from the mass conservation equation and the electric potential ($\vec{E} = -\nabla\phi$) is calculated from the charge conservation equation.

In IEF, the ionic strength changes with time until a final steady state is reached. Hence, the mobility of proteins and ampholytes is affected by the ionic strength during the IEF process. For biprotic ampholytes ($j = 1^+$, 0, 1^-), Onsager–Debye–Huckel theory is applied to obtain the corrected mobility of species (μ_{ij}) from the limiting mobility using Eq. (10). In addition, the activity coefficients shown in Eq. (14) are calculated using ionic strength at each time step to compute the mixed equilibrium constants in Eqs. (12) and (13). Finally, the ionic-strength-dependent effective mobility, $\langle\mu_i\rangle$, of each ampholyte is computed from Eq. (9) using the corrected mobility of the ampholyte species and the mixed equilibrium constants. The diffusion coefficient of biprotic ampholytes is calculated as $D_i = D_{i1^\pm} = RT/F|\mu_{i1^\pm}/z_{i1^\pm}| = RT/F|\mu_{i1^\pm}|$.

Table 1. Electrochemical properties of model proteins used in the IEF simulation[a)]

pK	Protein 1 (pI = 6.49)	Protein 2 (pI = 7.1)	Protein 3 (pI = 7.93)	Protein 4 (pI = 8.6)
pK_1	0.05	0.025	0.005	0.005
pK_2	2.6	3.6	4.2	4.2
pK_3	3	4	4.5	5.5
pK_4	3.25	4.25	5.25	5.8
pK_5	3.5	4.5	6.4	6.4
pK_6	5.45	6.45	6.45	7.45
pK_7	6.4	7.4	7.6	9
pK_8	8.3	8.3	9.5	10
pK_9	9	9	10	11.5
Z_0	4	3	3	3

a) The pI value of each protein is computed from dissociation (equilibrium) constants and valence of protein with all protons (Z_0) [30].

The diffusion coefficient of proteins is obtained from the literature and the radius of each protein is calculated by Stokes' Equation (Eq. (18)). The effective electrophoretic mobility of each protein is calculated as $\langle \mu_i \rangle = \overline{\omega}_i \langle z_i \rangle$, where $\overline{\omega}_i$ is obtained from Eqs. (15)–(18); the effective valence, $\langle z_i \rangle$, of each protein is estimated using Eq. (3). The effective mobility has a maximum value at the lowest ionic strength ($I_s = 0$), whereas it has a minimum value at the highest ionic strength ($I_s \to \infty$). At each time step, the ionic strength was updated in Eq. (16) to adjust the effective mobility of each protein.

This model neglects Joule heating because relatively smaller electric fields are used for separation. Electric field-induced electrokinetic flow is not considered here because, in most of our IEF experiments [4, 15], the channel is coated with methylcellulose or other chemicals to suppress electroosmosis.

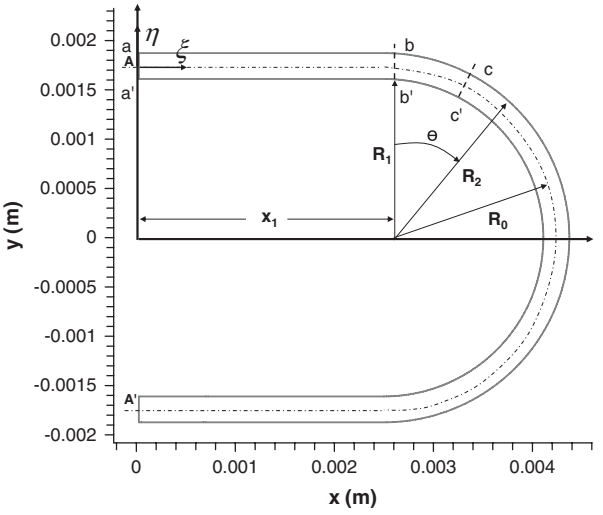

Figure 1. Schematic of a horseshoe microchannel. The section AA′ is the centerline of horseshoe channel. R_1 (1.516 mm) is the inner radius, R_2 (1.816 mm) is the outer radius and R_0 (1.666 mm) is the mean radius of the channel. Total mean length of the channel is 1 cm and the channel width is 300 μm. The anodic reservoir is located at location A, whereas the cathodic reservoir is located at A′.

4 Results and discussion

Mobility corrections on electrolytes and proteins have been investigated in the past [28, 29, 31]. Gas and his colleagues [28] used Onsager–Debye–Huckel theory to report the effect of ionic strength on the electrophoretic mobility of small ions such as background electrolyte in CZE. In their work, they showed that stronger ionic strength causes higher reduction in mobility of ions in electrophoretic process. Mosher *et al.* [31] presented the effect of ionic strength on protein behavior in IEF using the Debye–Huckel–Henry model. In addition, the effect of the ampholyte mobility correction on protein behavior was simulated in our previous paper [25]. Previous studies have only shown the effects of ionic strength on the mobility of proteins or ampholytes separately, but the effects of both (protein and ampholyte) mobility corrections on protein behavior have not been reported. In this study, mobility corrections for both proteins and ampholytes were considered in the numerical model to ascertain the effect of buffer ionic strength.

The 2-D finite volume method is used to study the band spreading induced by dispersion in a horseshoe microchannel during IEF. Details of the numerical scheme and boundary conditions are presented in our earlier publication [27]. The simulation was performed in the presence of 25 ampholytes to form a pH range of 6–9. Four model proteins, each having ten charge states, are focused in a horseshoe microchannel. The electrochemical data for proteins are listed in Table 1. The horseshoe channel with a 180° turn is depicted in Fig. 1. The angle of channel is defined in Fig. 1 such that the range of the turn angle varies from 0 to 180°. The anode is assigned at the upper left corner of the channel and the cathode is set at the lower left corner of the channel. The potential at the cathode is set at ground, whereas the potential at the anode is 300 V.

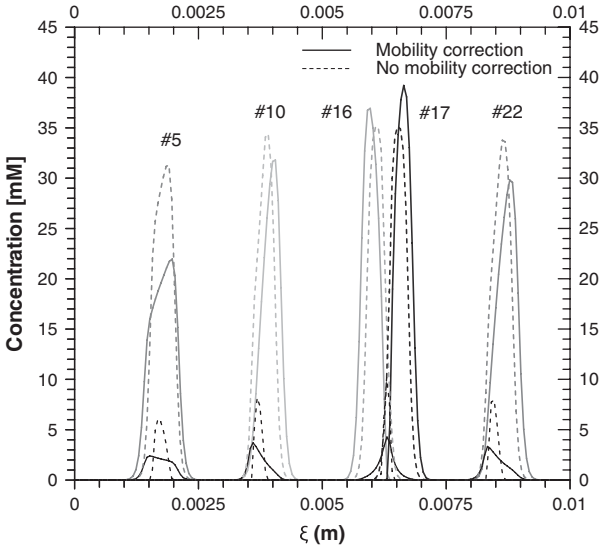

Figure 2. Comparison of focused-state behaviors of (selected) ampholytes and proteins without mobility corrections (dashed line) and with mobility corrections (solid line) of both protein and ampholyte mobilities. Concentration of proteins and ampholytes is presented by thick and thin lines, respectively. The limiting mobilities of each ampholyte are $-3E{-}04\ cm^2/V\,s$ and $3E{-}04\ cm^2/V\,s$ for negative and positive charge states, respectively. The ΔpK $(pK_2 - pK_1)$ for each ampholyte is 3. All proteins were assumed to have equal diffusion coefficient of $9.75E{-}11\ m^2/s$. The initial concentration of proteins and ampholytes are 1.5 and 0.15 mM, respectively.

4.1 Effects of mobility correction

The focused concentrations of four model proteins are presented in Fig. 2 to examine the effects of mobility corrections on protein behavior. The results were extracted at the channel centerline (along the ξ-axis) in Fig. 1. The simulation of IEF in a horseshoe microchannel was completed in less than 380 s at nominal electric field strength of 300 V/cm. Although 25 biprotic ampholytes are used in this simulation, five selected ampholytes (♯5, 10, 16, 17 and 22) close to model proteins are presented to illustrate the proteins' behavior at the final focusing time ($t = 380$ s).

The numerical results show that the focusing position of each protein is the same regardless of the mobility correction, but the focused shapes of the proteins are considerably affected by the mobility correction. When only the ampholyte correction is used in an IEF simulation, it induces slower movement of proteins in early-stage IEF, but the focused positions and concentrations are similar at the final stage of IEF [25]. However, including both (protein and ampholyte) mobility corrections produce significantly different heights in the protein concentrations. Furthermore, the focused position of a protein impacts the final focused shape of ampholyte(s). In Fig. 2, the pI value (p$I = 6.49$) of the protein 1 is closer to the pI value (p$I = 6.5$) of ampholyte ♯5, so the focused shape of the ampholyte ♯5 is less symmetric at the final focusing time. This effect of protein position on ampholyte shape is in agreement with previous results [25–27].

4.2 Dispersion in a horseshoe microchannel

Although the effect of turns on band spreading was studied in microchannels for linear electrokinetic transport, protein dispersion has not been reported in an IEF process for a 2-D-shaped geometry. In this paper, we illustrate the dispersion of proteins in IEF and discuss the difference between linear electrophoretic transport and non-linear IEF in a horseshoe microchannel. Two different stages are considered for the IEF process: gradient formation and protein focusing. During the gradient formation stage, two protein peaks are formed at both ends of the channel (for each protein), and these bands continue to move toward each other until a single band is formed. The focusing stage refers to the transport process between merging of two bands of each protein and formation of final focused band at their pI position.

Figure 3 presents snapshots of the concentration distribution of model protein 2 as it focuses. The gradient formation stage is shown in Figs. 3(A–D) where two bands of model protein 2 initially form at the electrodes and then coalesce at the protein's pI. The formation of these two bands is similar to earlier experimental and numerical IEF studies [4, 27, 30]. In Fig. 3B, the protein band near the cathode shows dispersion due to the turn, while the band near the anode has negligible dispersion at 35 s. At 48 s, both bands show some dispersion, but the protein near the cathode shows significantly more than that of the protein near the anode. The main reason for two different dispersions is the non-uniform electrophoretic velocities between the inner and outer edges of the channel (aka "racetrack effect") [18]. As a protein band traverses a turn, the protein molecules in the band migrate around the turn at different velocities under the action of electric field and this often results in excessive distortion of protein bands around the turn. In Fig. 3D, the two bands merge and form a single band around the protein's pI. Unlike linear electrophoresis, the width of the resulting protein band reduces considerably as it approaches focused-state near its pI due, in large part, to the self-sharpening properties of non-linear IEF. On the other hand, in a linear electrophoretic separation or electroosmotic flow, the band keeps spreading because linear electrophoresis inherently lacks the ability to self-sharpen after dispersion.

The focusing stage of protein 2 is shown in Figs. 3 (E and F). During the focusing stage, the mobilities of the two bands are reduced significantly as they approach the isoelectric point. If there is no bulk flow in the system, the velocities of two bands are nearly equal and opposite during this stage. Hence, these effects self-sharpen the dispersed bands in the horseshoe turn, and a highly focused band with very minimal dispersion can be obtained at the

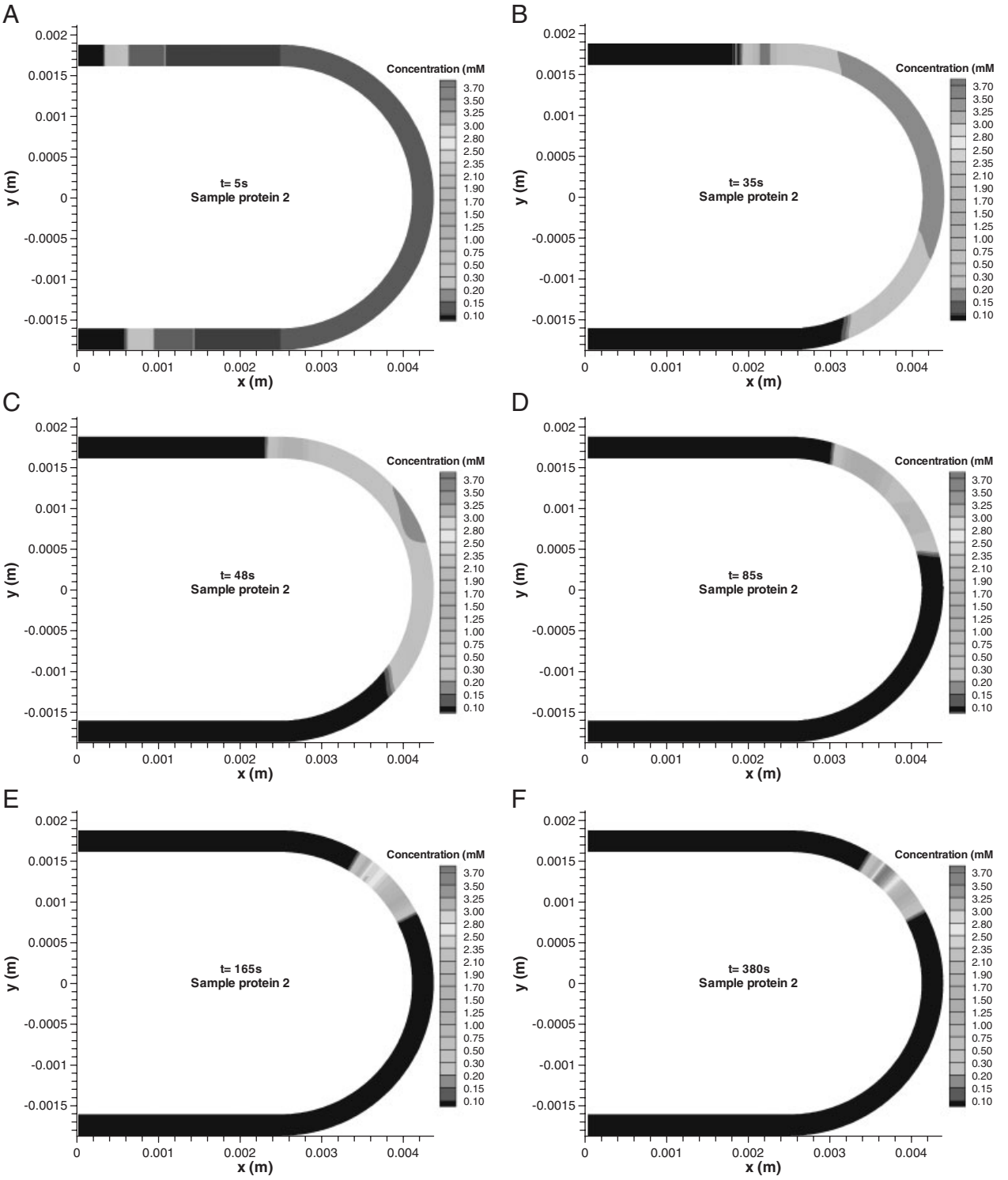

Figure 3. Concentration contours of model protein 2 at different times during IEF. (A)–(D) are obtained at gradient formation stage, whereas (E) and (F) are acquired at the final stage of focusing. Ampholyte-based IEF simulation was performed in a horseshoe microchannel for four model proteins in the presence of 25 ampholytes. Electrode voltages at anode and cathode are 300 and 0 V, respectively.

isoelectric point. This ampholyte-based IEF is completely different from linear electrophoretic techniques (ZE) where solute bands rapidly disperse during turns.

Figure 4 shows the transient evolution of all four proteins in a horseshoe channel. At 100 s, all proteins have moved near to their p*I* positions. Note that proteins 2

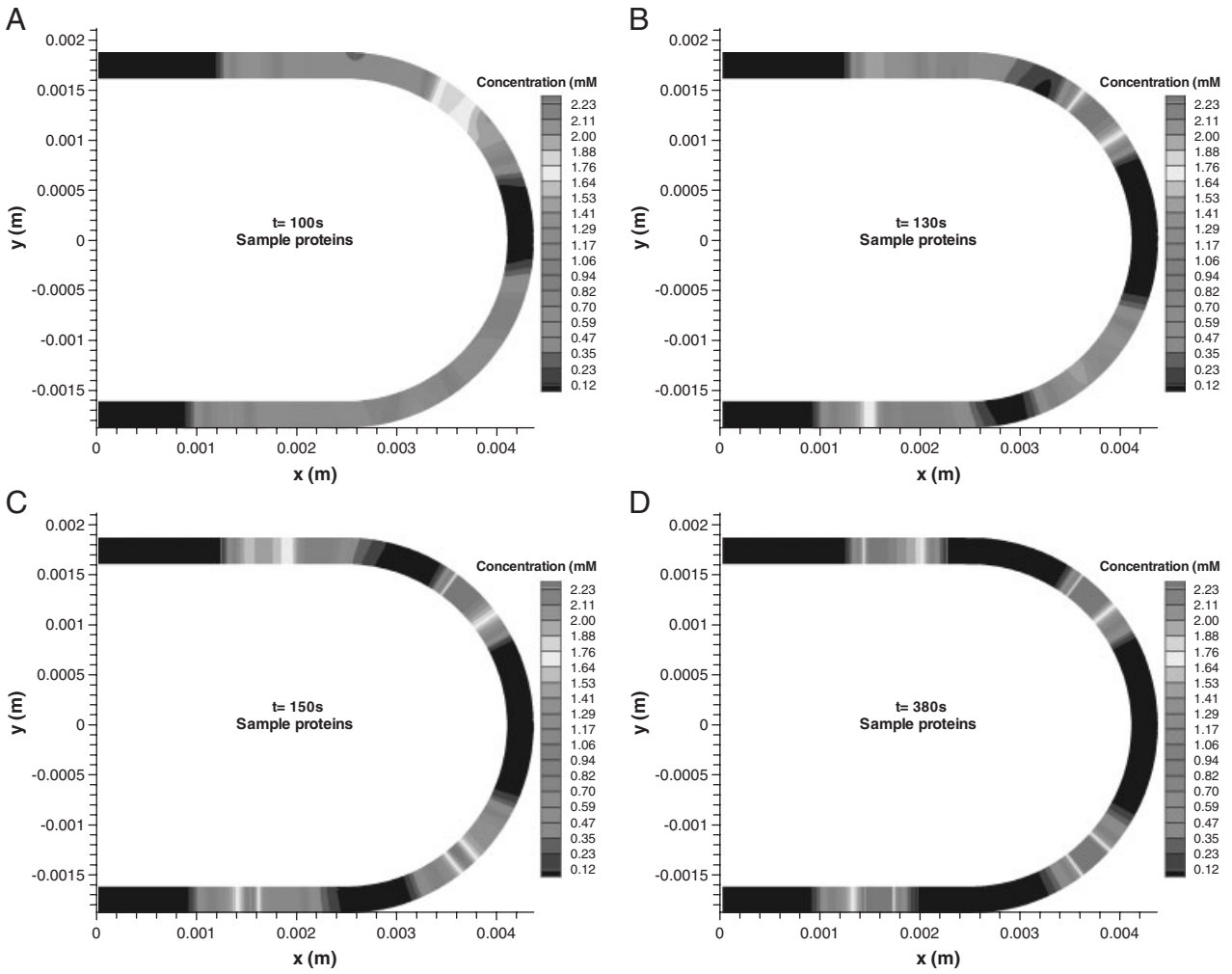

Figure 4. Concentration contours of all four model proteins during final stages of focusing. All simulation conditions remain the same as in Fig. 3.

and 3 (p*I*s = 7.1 and 7.93, respectively) form bands along the turn, whereas the proteins 1 and 4 (p*I*s = 6.49 and 8.6, respectively) form in the straight part of the horseshoe channel. At 130 and 150 s, all protein concentrations become constant across the transverse axis of the channel at their p*I*s. Finally, all proteins are focused with minimal dispersion by 380 s. In other words, in the focused-state, dispersion can be mitigated significantly and high-resolution bands can be formed regardless of the turn geometry.

In order to produce a quantitative estimate of the dispersion in IEF, the normalized variances of all proteins are presented in Fig. 5. The normalized variances are calculated using Eqs. (A3)–(A5) (see Supporting Information) after transforming the coordinate system from Cartesian (x, y) to a curvilinear (ξ,η) system for the concentration distribution. Figure 5A shows the normalized variance in the ξ-axis which is the direction of migration. The normalized variance starts at an initial value of about 92 as protein peaks start to form at the anodic and cathodic ends of the channel. The variance decreases linearly until a pair of protein peaks starts to merge near their isoelectric points during IEF. The simulation results show that the normalized variances of proteins (1–4) are different during the initial stage as shown in Fig. 5A.

The protein-to-protein variation is primarily related to their p*I* position and migration speed. For instance, the p*I* positions of proteins 1 and 4 are close to the anode and cathode respectively, whereas the p*I*s of proteins 2 and 3 are positioned in the turn region, which is located at the middle section of the horseshoe channel. For proteins 1 or 4, one protein peak is closer to the p*I* point and the other peak has to travel a long path before reaching the p*I* point. On the other hand, for proteins 2 and 3, both peaks move about the same length before reaching to their p*I* points. As the two peaks of proteins continuously move toward their isoelectric point, the variances of proteins 2 and 3 are initially less than that of proteins 1 and 4. After the protein peaks merge to a single band, their variances change very little (Fig. 5A) for all proteins.

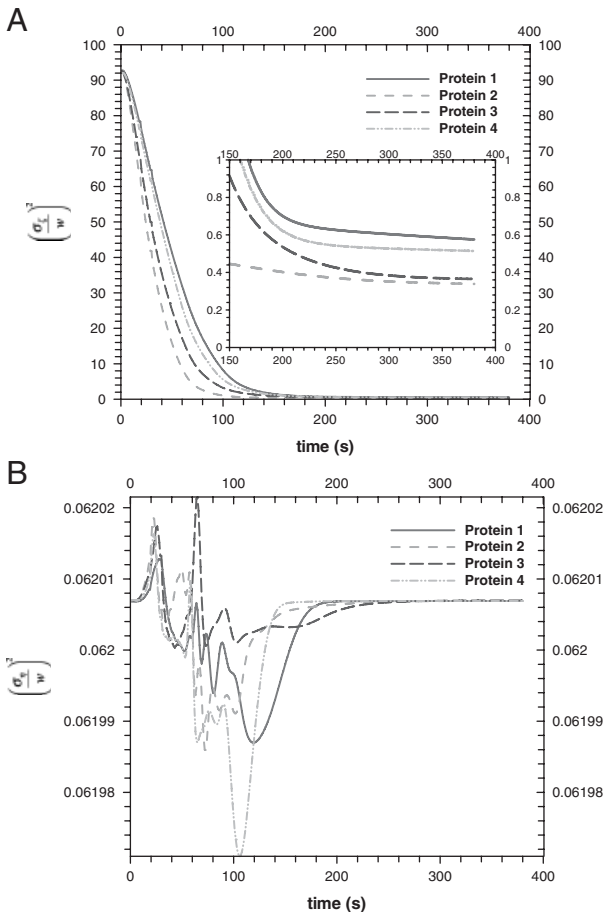

Figure 5. The normalized protein band dispersion in (A) streamwise direction and (B) cross-stream direction. The inset figure shows the dispersion during the final stages of focusing. Moment analysis is used to calculate the variances.

Figure 5B shows the normalized variance in the η-direction, which illustrates the race course effect. It is important to note that, for a straight channel, there is no dispersion in the cross-stream (lateral) direction and the lateral variance remains same at all times. In a horseshoe microchannel, the fluctuation of variances is related to the transient concentration variation across the channel. When voltages are applied at the channel ends, the concentration of protein fluctuates along the η-direction before the two peaks of protein focus at the p*I*. However, when the peaks are finally focused, the variance along the η-direction returns the same value of the initially uniform protein distribution.

Figure 6 shows how the dispersion is rearranged as protein 3 is focused near its p*I* position. When voltages are applied at the electrodes for IEF, the double peaks of the protein 3 are initially evolved at the anode and cathode. These double peaks of the protein 3 migrate toward its p*I* point and form one single band. At 120 s, the double peaks of the protein 3 come close to each other and at 140 s they start to merge. At 160 s, two peaks become tightly attached and form one straight band, which is radially smooth at longer times.

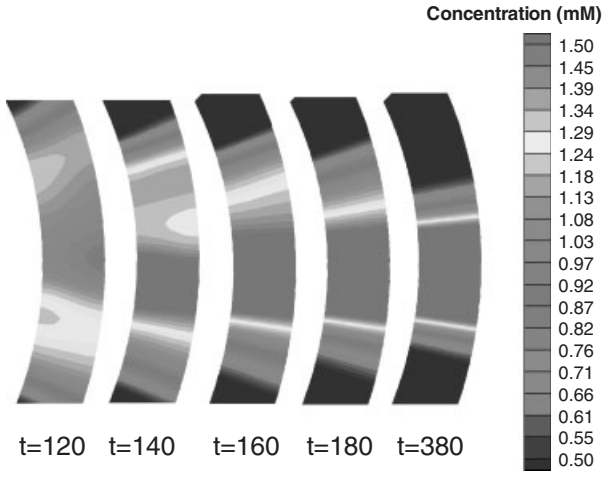

Figure 6. The rearrangement of protein 3 during final stages of focusing near the 180° turn angle. All time is in seconds.

5 Concluding remarks

In this paper, an IEF simulation was conducted to study dispersion of proteins in a horseshoe microchannel. Four model proteins are focused in a 1-cm-long horseshoe channel under an electric field of 300 V/cm. The pH gradient is formed in the presence of 25 ampholytes within a pH range of 6–9. The proteins are focused at 380 s in a nominal electric field of 300 V/cm. Numerical results show that mobility corrections have an important impact on the final focused concentration of proteins as well as ampholytes, but the focal points of the proteins are the same as those without the mobility correction. The ionic-strength-dependent mobility correction predicts significantly lower protein peak heights at focused-state than that of constant absolute mobility case.

Though various analytical and numerical approaches have been presented for band spreading in microchannel turns in electroosmotic flow, pressure-driven flow or linear electrophoresis, no study has reported band dispersion in a complex geometry during ampholyte-based IEF. In this study, normalized variances were calculated from numerical results using moments. Our numerical results show that protein band spreading is induced by a turn during the transient portion of IEF, but the dispersed bands focus with straight edges at final focusing state. This rearrangement of spreading band is unique compared with linear electrokinetic phenomena and is independent of channel position and channel shape. Hence, one can perform IEF in complex geometries without incorporating hyperturns.

This work was partly supported by the National Science Foundation under grant number CBET0626471. J. Shim acknowledges the support of Yeungnam University.

The authors have declared no conflict of interest.

6 References

[1] Righetti, P. G., *Isoelectric Focusing: Theory, Methodology and Applications*, Elsevier, Amsterdam 1983.

[2] Bier, M., Palusinski, O. A., Mosher, R. A., Saville, D. A., *Science* 1983, *219*, 1281–1287.

[3] Mao, Q., Pawliszyn, J., Thormann, W., *Anal. Chem.* 2000, *72*, 5493–5502.

[4] Cui, H., Horiuchi, K., Dutta, P., Ivory, C. F., *Anal. Chem.* 2005, *77*, 1303–1309.

[5] Everaerts, F. M., Beckers, J. L., Verheggen, Th. P. E. M., Isotachophoresis, in: *Journal of Chromatography Library*, vol. 6, Elsevier, Amsterdam 1976.

[6] Udseth, H. R., Loo, J. A., Smith, R. D., *Anal. Chem.* 1989, *61*, 228–232.

[7] Cui, H., Dutta, P., Ivory, C. F., *Anal. Chem.* 2007, *79*, 1456–1465.

[8] Cheng, Y. F., Dovichi, N. J., *Science* 1988, *242*, 562–564.

[9] Rose, D. J., Jorgenson, J. W., *Anal. Chem.* 1988, *60*, 642–648.

[10] Wey, A. B., Wolfgang, T., *J. Chromatogr. A* 2001, *916*, 225–238.

[11] Yang, C., Zhang, L., Liu, H., Zhang, W., Zhang, Y., *J. Chromatogr. A* 2003, *1018*, 97–103.

[12] Herr, A. E., Molho, J. I., Drouvalakis, K. A., Mikkelsen, J. C. *et al.*, *Anal. Chem.* 2003, *75*, 1180–1187.

[13] Bodor, R., Madajova, V., Kaniansky, D., Masar, M. *et al.*, *J. Chromatogr. A* 2001, *916*, 155–165.

[14] Mohan, D., Lee, C. S., *Electrophoresis* 2002, *23*, 3160–3167.

[15] Cui, H., Horiuchi, K., Dutta, P., Ivory, C. F., *Anal. Chem.* 2005, *77*, 7878–7886.

[16] Culbertson, C. T., Jacobson, S. C., Ramsey, J. M., *Anal. Chem.* 1998, *70*, 3781–3789.

[17] Griffiths, S., Nilson, R. H., *Anal. Chem.* 2000, *72*, 5473–5482.

[18] Ghosal, S., *Annu. Rev. Fluid Mech.* 2006, *38*, 309–338.

[19] Tang, G. Y., Yang, C., Gong, H. Q., Chai, J. C., Lam, Y. C., *Anal. Chim. Acta* 2006, *561*, 138–149.

[20] De Leebeeck, A., Sinton, D., *Electrophoresis* 2006, *27*, 4999–5008.

[21] Knox, J., *Chromatographia* 1988, *25*, 203–213.

[22] Wang, Y., Lin, Q., Mukherjee, T., *Lab Chip* 2004, *4*, 625–631.

[23] Sun, Y., Kwok, Y. C., Nguyen, N. T., *Electrophoresis* 2007, *28*, 4765–4768.

[24] Paschkewitz, J. S., Molho, J. I., Xu, H., Bharadwaj, R., Park, C. C., *Electrophoresis* 2007, *28*, 4561–4571.

[25] Shim, J., Dutta, P., Ivory, C. F., *Electrophoresis* 2008 *29*, 1026–1035.

[26] Shim, J., Dutta, P., Ivory, C. F., *J. Nanosci. Nanotechnol.* 2008, *8*, 3719–3828.

[27] Shim, J., Dutta, P., Ivory, C. F., *Electrophoresis* 2007, *28*, 572–586.

[28] Zuskova, I., Novotna, A., Vcelakova, K., Gas, B., *J. Chromatogr. B* 2006, *841*, 129–134.

[29] Vcelakova, K., Zuskova, I., Kenndler, E., Gas, B., *Electrophoresis* 2004, *25*, 309–317.

[30] Mosher, R. A., Saville, D. A., Thormann, W., *The Dynamics of Electrophoresis*, VCH, Weinheim 1992.

[31] Mosher, R. A., Dewey, D., Thormann, W., Saville, D. A., Bier, M., *Anal. Chem.* 1989, *61*, 362–366.

[32] Moody, T. P., Kingsbury, J. S., Durant, J. A., Wilson, T. J. *et al.*, *Anal. Biochem.* 2005, *336*, 243–252.

